Journal of Sound and Vibration (2000) **238**(5), 853–867
doi:10.1006/jsvi.2000.3136, available online at http://www.idealibrary.com on IDEAL®

ONE-DIMENSIONAL PREDICTION OF THE ACOUSTIC WAVES GENERATED IN A MULTILAYER VISCOELASTIC BODY BY MICROWAVE IRRADIATION

C. Bacon, B. Hosten and E. Guilliorit

Laboratoire de Mécanique Physique, Université Bordeaux 1, *UMR* 5469 *CNRS*
351, *cours de la Libération*, 33405 *Talence Cedex*, *France. E-mail*: *bacon@lmp.u-bordeaux.fr*

(*Received* 7 *February* 2000, *and in final form* 22 *May* 2000)

A one-dimensional method to predict the acoustic waves generated by a rapid thermal expansion in a multilayer viscoelastic body (rod or plate) is presented. In particular, the method can predict the acoustic waves generated by microwave irradiation. The temperature rise in each layer is assumed to be known. The solution is validated experimentally with a rod made with two different materials and irradiated by a pulsed microwave. An example of application is given in the case of the acoustic wave generation in a metallic medium by means of the microwave irradiation of an absorbing layer.

1. INTRODUCTION

Many investigators have studied the auditory sensations produced in men irradiated with electromagnetic microwaves. Indeed, pulsed microwaves have been heard as buzzing, hissing or knocking sounds by radar operators since radar was invented during World War II. In their comprehensive review about this subject, Chou and Guy [1] wrote: "When the observers first told their coworkers in the Laboratory of their hearing experiences, they encountered skepticism and rather pointed questions about their mental health". Consequently, the phenomenon of acoustic wave generation by electromagnetic microwaves has been studied particularly for its biological effects since the 1960s.

Several mechanisms have been suggested to explain the phenomenon of microwave hearing, i.e., radiation pressure, electrostriction or thermal expansion. Numerous psychological, physiological, behavioral and physical studies have been conducted to conclude that the auditory sensation produced by electromagnetic microwaves is mainly due to the thermal expansion mechanism, first proposed by Foster and Finch [2] in 1974: the microwave energy is absorbed and converted into thermal energy, which causes the irradiated material to expand in accordance with its thermoelastic properties. Thus, the acoustic waves are produced by a sudden heating of the irradiated material.

A great number of theoretical papers [3–7] treat the acoustic waves resulting from thermal expansion produced in an elastic body by sudden heating due to electromagnetic energy penetration (optical penetration of laser pulse or microwave irradiation). Michaels [3] first considered elastic wave generation by rapid thermal expansion at the end of one-dimensional bodies. The solution was illustrated by an approximated convenient function representing the temperature distribution but which did not satisfy the heat

0022-460X/00/500853 + 15 $35.00/0

conduction equation. This problem was solved by White [4]. He investigated several transient heating conditions. The problem of an input energy flux varying harmonically with time was treated in detail. Later, Borth and Cain [6] presented a theoretical study taking thermal expansion but also electrostriction and radiation pressure into account for an elastic body. They concluded that thermal expansion was considerably more effective than either electrostriction or radiation pressure in converting electromagnetic energy to acoustic energy.

In the studies cited above, it is generally considered that the spatial profile of the temperature is exponential. It is difficult to extend the analytical results obtained to other temperature distributions. Moreover, the material is assumed to be elastic and so the viscoelastic effects cannot be investigated.

For many materials, contrary to the case of laser-generated ultrasounds, the absorption is very much lower and the depth of wave generation is more important in the case of microwave irradiation. Consequently, any interface in the specimen may contribute to the wave generation even if it is far from the irradiated surface [8, 9]. For a specimen made of several layers with different materials (a laminated plate, for instance), a method must be developed to predict the acoustic waves generated by a rapid microwave irradiation. Indeed, in this case, the temperature rise due to the electromagnetic absorption may be different in each layer and the acoustic waves may be generated at each interface and, also, all over the specimen if a gradient of the temperature rise exists in the layers. Moreover, these waves will be reflected at each interface owing to the different mechanical properties.

Some one-dimensional [11] or two-dimensional [12] models have been proposed to analyze the acoustic response of structures made of two elastic layers. The aim of the current paper is to present a one-dimensional numerical method to predict the acoustic waves generated by a rapid thermal expansion in a viscoelastic body made of any number of uniform layers. In each layer, it is assumed that the temperature rise is known. Any temperature profile will be able to be investigated by dividing the body into a sufficient number of uniform segments with linear temperature profiles. The case of an exponential temperature profile will also be investigated.

The method will be developed in section 2. Then, an experimental validation will be presented, obtained by means of an instrumented rod made of two different materials irradiated by microwaves. Afterwards, an example of application will be shown in the case of the acoustic wave generation in a metallic medium by the microwave irradiation of an absorbing layer.

2. THEORY

In this section, the general case for any profile of the temperature rise will be first treated. The irradiated body will be divided into several segments. The solution obtained will involve the knowledge of a function $\tilde{\varepsilon}_p(z, \omega)$ (in the Fourier domain) which depends on the profile of the temperature rise in each segment. Afterwards, the particular cases of a linear profile and an exponential profile of the temperature rise will be treated.

2.1. GENERAL CASE

Consider an elastic or viscoelastic body which can be divided into $n-1$ segments $\#j$ ($z_j \leqslant z \leqslant z_{j+1}$ where z is the axial coordinate, see Figure 1). The length of the segment $\#j$ is L_j. In each segment, the mechanical characteristics, the mass density ρ_j and the

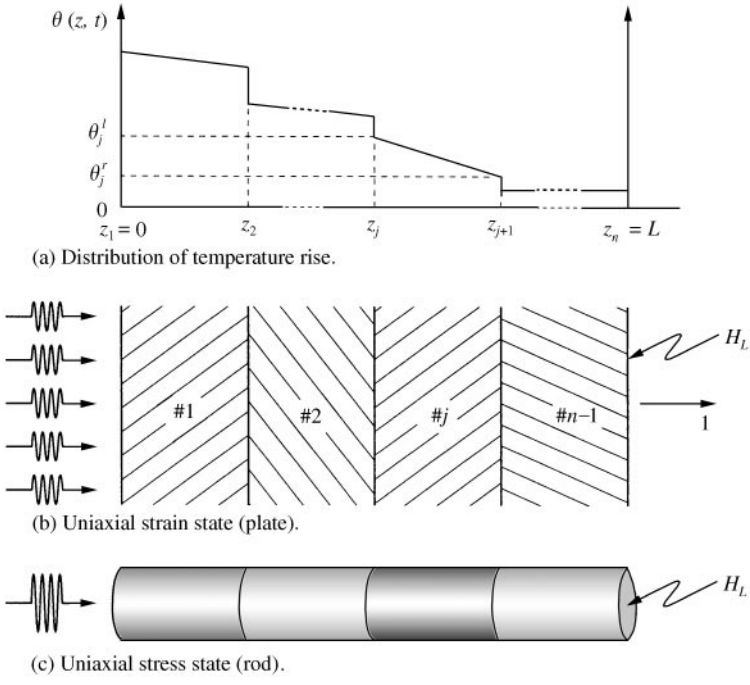

Figure 1. Viscoelastic body divided into $n-1$ segments $\#j$. (a) distribution of temperature rise; (b) uniaxial strains state (plate); (c) uniaxial stress state (rod).

cross-sectional area A_j are uniform. The co-ordinate at the first end of the body is $z_1 = 0$ and the coordinate at the second end is $z_n = L$. The free surface $z = 0$ is irradiated uniformly by an electromagnetic wave. Owing to the electromagnetic absorption, a temperature rise $\theta(z, t)$ occurs inside the body (t is the time). The temperature is not necessarily continuous.

Two one-dimensional problems can be treated together: the case of a uniaxial strain state [see Figure 1(b)] and the case of a uniaxial stress state [see Figure 1(c)]. A uniaxial strain state concerns a problem where the lateral dimensions are important compared to the thickness of the body. In this case, one can choose $A_j = 1$ for any segment. It can be noticed that it is easy to irradiate a large surface uniformly by means of microwaves while it is quite difficult with a laser. The stress state can be considered uniaxial in a rod when the lateral dimensions are much smaller than the wavelengths. In both cases, the Fourier transforms, $\tilde{\sigma}(z, \omega)$ and $\tilde{u}(z, \omega)$, of the normal stress $\sigma(z, t)$ and the axial displacement $u(z, t)$ in segment $\#j$, respectively, are related by (a list of nomenclature is given in Appendix A)

$$\frac{\partial}{\partial z}\tilde{\sigma}(z, \omega) = -\rho_j \omega^2 \tilde{u}(z, \omega), \tag{1}$$

where the angular frequency ω is related to the frequency v by $\omega = 2\pi v$. In the case of a uniaxial strain state, the linear viscoelastic constitutive law of the segment $\#j$ can be expressed in the frequency domain as

$$\tilde{\sigma}(z, \omega) = C_{11}^{*j}\tilde{\varepsilon}(z, \omega) - (C_{11}^{*j}\alpha_1^j + C_{12}^{*j}\alpha_2^j + C_{13}^{*j}\alpha_3^j)\tilde{\theta}(z, \omega), \tag{2}$$

where C_{1k}^{*j} are the components of the complex stiffness matrix in segment $\#j$ (the index 1 denotes the orthotropic axis in the z direction, 2 and 3 the other two orthotropic axes), α_k^j are the coefficients of linear thermal expansion in the orthotropic directions, and $\tilde{\varepsilon}(z, \omega)$ and $\tilde{\theta}(z, \omega)$ the Fourier transforms of the longitudinal strain and the temperature rise above the initial temperature respectively. In the case of a uniaxial stress state, this relation becomes

$$\tilde{\sigma}(z, \omega) = E_j^* \tilde{\varepsilon}(z, \omega) - E_j^* \alpha_1^j \tilde{\theta}(z, \omega), \tag{3}$$

where E_j^* is the complex Young's modulus in the z direction. To facilitate the analysis, the temperature distribution will be assumed to be independent of the mechanical state of the material. From equations (1) and (2) or equations (1) and (3), it can be demonstrated that the Fourier transforms of the axial displacement in segment $\#j$ can be calculated if the longitudinal strain and the temperature rise are known, i.e.,

$$\tilde{u}(z, \omega) = \frac{1}{(\omega S_j^*)^2} \left[\beta_j \frac{\partial \tilde{\theta}(z, \omega)}{\partial z} - \frac{\partial \tilde{\varepsilon}(z, \omega)}{\partial z} \right], \tag{4}$$

where the complex slowness $S_j^* = S_j' - \mathrm{i}S_j''$ and the expansion coefficient β_j are given by, for a uniaxial strain state,

$$S_j^{*2} = \frac{\rho_j}{C_{11}^{*j}} \quad \text{and} \quad \beta_j = \frac{C_{11}^{*j}\alpha_1^j + C_{12}^{*j}\alpha_2^j + C_{13}^{*j}\alpha_3^j}{C_{11}^{*j}}, \tag{5}$$

and for a uniaxial stress state,

$$S_j^{*2} = \frac{\rho_j}{E_j^*} \quad \text{and} \quad \beta_j = \alpha_1^j. \tag{6}$$

In both cases, equations (2) and (3) become

$$\tilde{\sigma}(z, \omega) = \frac{\rho_j}{S_j^{*2}} [\tilde{\varepsilon}(z, \omega) - \beta_j \tilde{\theta}(z, \omega)]. \tag{7}$$

The axial particle velocity $\tilde{v}(z, \omega)$ and the axial acceleration $\tilde{a}(z, \omega)$ are given by

$$\tilde{v}(z, \omega) = \mathrm{i}\omega \tilde{u}(z, \omega), \quad \tilde{a}(z, \omega) = -\omega^2 \tilde{u}(z, \omega). \tag{8}$$

In the hypothesis of small strains, the longitudinal strain is related to the axial displacement by $\varepsilon(z, t) = \partial u(z, t)/\partial z$. Consequently, equation (1) becomes

$$\frac{\partial^2 \tilde{\varepsilon}(z, \omega)}{\partial z^2} + \omega^2 S_j^* \tilde{\varepsilon}(z, \omega) - \beta_j \frac{\partial^2 \tilde{\theta}(z, \omega)}{\partial z^2} = 0. \tag{9}$$

The general solution of this equation can be written as

$$\tilde{\varepsilon}(z, \omega) = \tilde{P}_j(\omega) \mathrm{e}^{-\mathrm{i}\omega S_j^*(z - z_j)} + \tilde{N}_j(\omega) \mathrm{e}^{+\mathrm{i}\omega S_j^*(z - z_j)} + \tilde{\varepsilon}_p(z, \omega), \tag{10}$$

where the functions $\tilde{P}_j(\omega)$ and $\tilde{N}_j(\omega)$ are the Fourier transforms of the strains at $z = z_j$ due to the waves travelling in the directions of increasing and decreasing z, respectively, if the

function $\tilde{\varepsilon}_p(z, \omega)$ equals zero. The function $\tilde{\varepsilon}_p(z, \omega)$ depends on the spatial profile of the temperature rise function $\tilde{\theta}(z, \omega)$ in segment $\#j$. Two different expressions of this function will be given in the cases of a linear profile and an exponential profile of the temperature rise.

At this stage, the purpose is to find the relationship between the normal force and the acceleration at cross-section z_j and these two quantities at cross-section z_{j+1}. There is continuity of these two quantities at each interface between two segments.

By writing the normal force $\tilde{F}(z, \omega)$ and the acceleration $\tilde{a}(z, \omega)$ at $z = z_j$ and $z = z_{j+1}$ with the help of equations (4), (7), (8) and (10), $\tilde{P}_j(\omega)$ and $\tilde{N}_j(\omega)$ can be eliminated. Then, one obtains

$$\begin{bmatrix} \tilde{F}_{j+1} \\ \tilde{a}_{j+1} \end{bmatrix} = P^{(j)} \begin{bmatrix} \tilde{F}_j \\ \tilde{a}_j \end{bmatrix} + G^{(j)}, \tag{11}$$

where the components of the matrix $P^{(j)}$ and the vector $G^{(j)}$ are defined by

$$P^{(j)} = \begin{bmatrix} c & \dfrac{\rho_j A_j}{\omega S_j^*} s \\ \dfrac{\omega S_j^*}{\rho_j A_j} s & c \end{bmatrix}, \tag{12}$$

$$G^{(j)} = \begin{bmatrix} \dfrac{A_j \rho_j}{S_j^{*2}} \left[(\beta_j \tilde{\theta}_j^l - \tilde{\varepsilon}_p^l) c - \beta_j \tilde{\theta}_j^r + \dfrac{s}{\omega S_j^*} \left(\beta_j \dfrac{\partial \tilde{\theta}}{\partial z}\bigg|_{z_i} - \dfrac{\partial \tilde{\varepsilon}_p}{\partial z}\bigg|_{z_j} \right) + \tilde{\varepsilon}_p^r \right] \\ \dfrac{1}{S_j^{*2}} \left[(\tilde{\varepsilon}_p^l - \beta_j \tilde{\theta}_j^l) \omega S_j^* s - \beta_j \dfrac{\partial \tilde{\theta}}{\partial z}\bigg|_{z_{j+1}} + c \left(\beta_j \dfrac{\partial \tilde{\theta}}{\partial z}\bigg|_{z_i} - \dfrac{\partial \tilde{\varepsilon}_p}{\partial z}\bigg|_{z_j} \right) + \dfrac{\partial \tilde{\varepsilon}_p}{\partial z}\bigg|_{z_{j+1}} \right] \end{bmatrix}, \tag{13}$$

where $c = \cos(\omega S_j^* L_j)$ and $s = \sin(\omega S_j^* L_j)$. $\tilde{\theta}_j^l = \tilde{\theta}(z_j, \omega)$ and $\tilde{\theta}_j^r = \tilde{\theta}(z_{j+1}, \omega)$ are the temperature rise at the left and right ends of segment $\#j$. The frequency functions $\tilde{\varepsilon}_p^l$ and $\tilde{\varepsilon}_p^r$ equal $\tilde{\varepsilon}_p(z_j, \omega)$ and $\tilde{\varepsilon}_p(z_{j+1}, \omega)$ respectively.

It can be noticed that the matrix $P^{(j)}$ is related to the wave propagation whereas the vector $G^{(j)}$ is related to the wave generation due to thermal expansion. Only $G^{(j)}$ depends on the spatial profile of the temperature rise in each segment. From equation (11), owing to the continuity of the normal force and acceleration, it can be shown that

$$\begin{bmatrix} \tilde{F}_j \\ \tilde{a}_j \end{bmatrix} = S^{(j)} \begin{bmatrix} \tilde{F}_1 \\ \tilde{a}_1 \end{bmatrix} + T^{(j)}, \quad j \geqslant 2 \quad \text{where} \begin{Bmatrix} S^{(j)} = P^{(j-1)} S^{(j-1)}, S^{(2)} = P^{(1)} \\ T^{(j)} = P^{(j-1)} T^{(j-1)} + G^{(j-1)}, T^{(2)} = G^{(1)} \end{Bmatrix}. \tag{14}$$

Consequently, the normal force and the acceleration at both ends of the irradiated body are linked together by the matrix $S^{(n)}$ and the vector $T^{(n)}$. Then, the determination of the acceleration at $z = L$ (for instance) involves the knowledge of the boundary conditions. The end at $z = 0$ is free. Consequently, the normal force at $z = 0$ must be zero, i.e., $\tilde{F}_1 = 0$. For $z > L$, it is considered that there is no temperature rise. The function $H_L(\omega) = \tilde{F}(L, \omega)/\tilde{a}(L, \omega)$ is supposed to be known (for instance, see equation (24) in the case of an accelerometer or equation (25) in the case of a semi-infinite medium). With the help of these boundary conditions and equation (14), the acceleration at $z = L$ is

$$\tilde{a}(L, \omega) = \tilde{a}_n = \frac{S_{22}^{(n)} T_1^{(n)} - S_{12}^{(n)} T_2^{(n)}}{H_L S_{22}^{(n)} - S_{12}^{(n)}}. \tag{15}$$

From this acceleration, the acceleration at $z = 0$ can be derived:

$$\tilde{a}(0, \omega) = \tilde{a}_1 = \frac{\tilde{a}(L, \omega) - T_2^{(n)}}{S_{22}^{(n)}}. \tag{16}$$

2.2. SEGMENTS WITH A LINEAR PROFILE OF THE TEMPERATURE RISE

Now consider segment $\#j$ of the body where it can be assumed that the temperature rise varies linearly with the axial coordinate z (see Figure 1). Then, the Fourier transform of the temperature rise at z between z_j and z_{j+1} is given by

$$\tilde{\theta}(z, \omega) = \tilde{\theta}_j^l(\omega) + z \cdot \left.\frac{\partial \tilde{\theta}}{\partial z}\right|_j (\omega) \quad \text{with} \quad \left.\frac{\partial \tilde{\theta}}{\partial z}\right|_j (\omega) = \frac{\tilde{\theta}_j^r(\omega) - \tilde{\theta}_j^l(\omega)}{L_j}. \tag{17}$$

In the case where the last term of equation (9) is zero (uniform or linear temperature along the z-axis), the general solution of this equation can be easily found:

$$\tilde{\varepsilon}(z, \omega) = \tilde{P}_j(\omega) e^{-i\omega S_j^*(z - z_j)} + \tilde{N}_j(\omega) e^{+i\omega S_j^*(z - z_j)} \quad \text{with } \tilde{\varepsilon}_p(z, \omega) = 0. \tag{18}$$

From equation (13), the vector $G^{(j)}$ can be calculated for this particular case. The solution is

$$G^{(j)} = \begin{bmatrix} \dfrac{A_j \rho_j \beta_j}{S_j^{*2}} \left(\tilde{\theta}_j^l c - \tilde{\theta}_j^r + \dfrac{s}{\omega S_j^*} \left.\dfrac{\partial \tilde{\theta}}{\partial z}\right|_j \right) \\ \dfrac{\beta_j \omega}{S_j^*} \left(- \tilde{\theta}_j^l s + \left.\dfrac{\partial \tilde{\theta}}{\partial z}\right|_j \dfrac{c - 1}{\omega S_j^*} \right) \end{bmatrix}. \tag{19}$$

2.3. SEGMENTS WITH AN EXPONENTIAL PROFILE OF THE TEMPERATURE RISE

In each segment $\#j$, it is now assumed that the temperature rise follows an exponential decrease in the z-direction along the irradiated body as

$$\theta(z, t) = K_j(t) e^{-a_j(z - z_j)} \quad \text{or} \quad \tilde{\theta}(z, \omega) = \tilde{K}_j(\omega) e^{-a_j(z - z_j)}. \tag{20}$$

In this case, the function $\tilde{\varepsilon}_p(z, \omega)$ is given by

$$\tilde{\varepsilon}_p(z, \omega) = \frac{\beta_j a_j^2}{a_j^2 + \omega^2 S_j^{*2}} \tilde{K}_j(\omega) e^{-a_j(z - z_j)}. \tag{21}$$

Consequently, from equation (13), the vector $G^{(j)}$ becomes

$$G^{(j)} = \begin{bmatrix} \dfrac{A_j \rho_j \beta_j \tilde{K}_j \omega^2}{a_j^2 + \omega^2 S_j^{*2}} \left(c - \dfrac{a_j s}{\omega S_j^*} - e^{-a_j L_j} \right) \\ \dfrac{\beta_j \tilde{K}_j \omega^2}{a_j^2 + \omega^2 S_j^{*2}} (-\omega S_j^* s + a_j e^{-a_j L_j} - a_j c \end{bmatrix}. \tag{22}$$

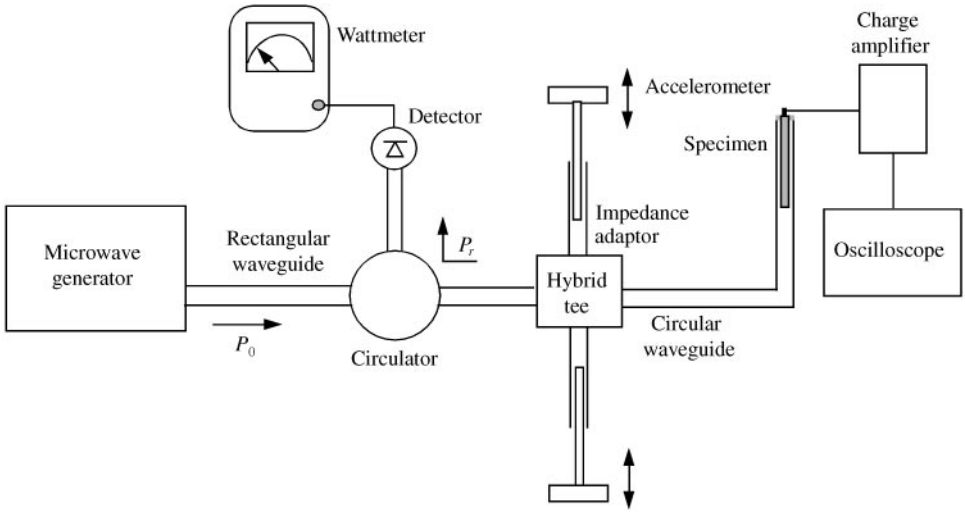

Figure 2. Set-up to generate and acquire acoustic waves.

3. EXPERIMENTAL VALIDATION

An experimental validation has been performed on a rod made of two different materials and submitted to a time-gated microwave irradiation. The materials are chosen so that their mechanical characteristics are quite different and the temperatures reached in each one are easily determined.

3.1. EXPERIMENTAL SET-UP

The time-gated electromagnetic microwaves are produced by a magnetron at 9·5 GHz (see Figure 2).

The power is of the order of 5·5 kW. The pulsewidth τ is 1·2 μs. The repetition rate is chosen sufficiently low in order to avoid the overlap between two consecutive records. First, the electromagnetic waves propagate in a rectangular waveguide. The incident power, P_0, which arrives in the circulator, is sent towards the specimen. To obtain the maximum power, an impedance adaptor is adjusted in order to get the minimum reflected power measured with a wattmeter. It is made up of a hybrid tee associated to two sliding short circuits. The last part of the waveguide (where the specimen is put) is circular with a diameter of 24 mm. The microwaves propagate in the TE_{11} fundamental mode in this circular waveguide.

The specimen rod, with a diameter of 15·5 mm, is made with a rod of PVC having a length of 10 cm and a rod of aluminium alloy having the same length (see Figure 3). The rods are glued together at one end.

A piezoelectric accelerometer (Brüel & Kjaer 4371) is attached to the end of the aluminium alloy rod by means of a very thin layer of ultrasonic couplant. Its mass m is 11 g and its charge sensitivity is 1·021 pC/ms^{-2}. The signal from the accelerometer is amplified by a charge amplifier (Brüel & Kjaer 2525). The amplified acceleration signals are recorded by a digital oscilloscope (LeCroy 9310). The signals are averaged on 10 sweeps in order to eliminate the electronic noise. Then, the signals are transferred to a computer for processing.

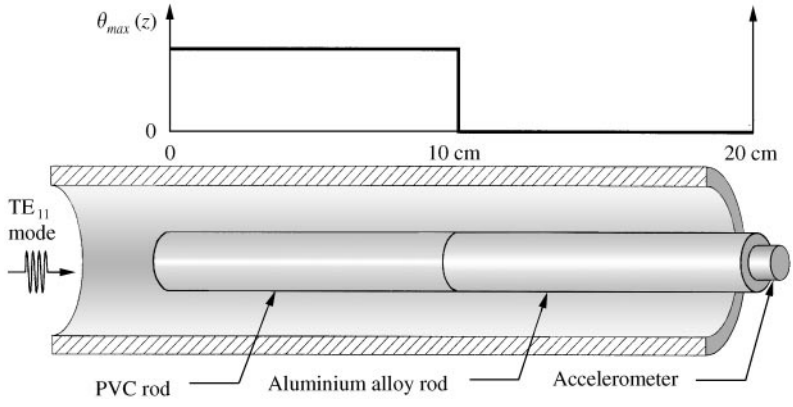

Figure 3. Maximum temperature rise in the PVC and the aluminium alloy rods.

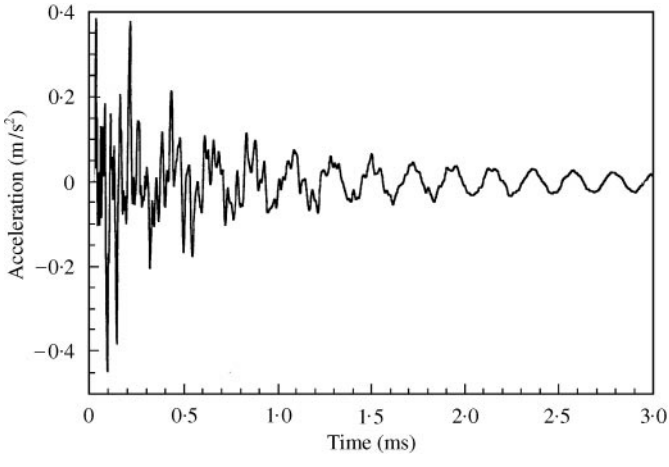

Figure 4. Experimental acceleration signal.

3.2. RESULTS

For the configuration described above, the acceleration of the rod end has been measured. The signal is plotted in Figure 4.

Since the mounted resonance frequency of the accelerometer is approximately 42 kHz and the experimental signal is not filtered, it is more convenient to compare the experimental and the theoretical spectra in the frequency range of accelerometer. For the determination of the theoretical acceleration spectrum, the following assumptions have been made.

The materials have been chosen so that the temperature profile can be easily predicted. The maximum temperature rise in the PVC rod can be supposed to be uniform while the temperature rise in the aluminium alloy rod is zero since this material is reflective for the microwaves. The value of the maximum temperature θ_{max} in the PVC has been evaluated by comparing the maximum values in the moduli of the theoretical and the experimental acceleration spectra. If the test duration is short, heat conduction can be ignored. Consequently, it can be assumed with sufficient accuracy that the PVC temperature rise $\theta(t)$

increases linearly during the pulsewidth ($0 < t < \tau$) and remains constant afterwards. Thus the temperature rise is

$$\theta(t) = \theta_{max} r(t) \quad \text{with } r(t) = \begin{cases} 0 & \text{for } t \leqslant 0, \\ t/\tau & \text{for } 0 < t < \tau, \\ 1 & \text{for } t \geqslant \tau. \end{cases} \tag{23}$$

The rod is instrumented with an accelerometer having a mass m at the end $z = L$. Thus, the normal force at this end is related to the axial velocity by

$$\tilde{F}(L, \omega) = -Z_a \tilde{v}(L, \omega) \quad \text{or} \quad H_L = \mathrm{i} Z_a/\omega, \tag{24}$$

where Z_a is the mechanical impedance of the accelerometer. At low frequencies, the accelerometer can be assumed to be a rigid mass. Then, its mechanical impedance is given by $Z_a = \mathrm{i}m\omega$.

The mass density and the coefficient of linear thermal expansion of the PVC are $1\,440\ \mathrm{kg/m^3}$ and $80 \times 10^{-6}/^{\circ}\mathrm{C}$ respectively. The complex slowness of the PVC have been obtained experimentally by irradiating a PVC rod having a length of 20 cm and instrumented with an accelerometer. The method used permits the determination of chosen parameters by a numerical minimization of the absolute difference between the experimental and the theoretical acceleration spectra [9, 10]. In the present case, the complex slowness has been evaluated by assuming that the profile of the temperature rise is exponential. Thus, solution (22) has been used for the vector $G^{(1)}$ with a single segment. The real part and the imaginary part of the complex slowness obtained are $S' = 599\ \mu\mathrm{s/m}$ and $S'' = 10\ \mu\mathrm{s/m}$ approximately. The exponential decrease has been found to be quite low since the PVC is a low-absorbing material for the microwaves. In the presence of damping, the real part of the slowness must depend on the frequently theoretically. However, owing to impact tests on a long instrumented PVC rod [9] and since the imaginary part is relatively low, it has been verified that the assumption of a constant slowness gives accurate results in the frequency range of the accelerometer.

The mass density and the slowness of the aluminium alloy are $2\,800\ \mathrm{kg/m^3}$ and $195\ \mu\mathrm{s/m}$ respectively. The experimental and the theoretical acceleration spectra are plotted in Figure 5. The theoretical acceleration spectrum has been calculated by using equation (15) with solution (19) for the vector $G^{(j)}$.

The comparison of both spectra shows a good agreement, particularly in the frequency range of the accelerometer up to about 10 kHz where the manufacturer gives a measurement error less than 10%. The maximum temperature rise evaluated in the PVC rod is about $8 \times 10^{-5}{}^{\circ}\mathrm{C}$. In the frequency range of Figure 5, the assumption of a constant temperature rise in the PVC is a good choice even if a small part of the incident electromagnetic wave is reflected by the aluminium alloy rod. At higher frequencies, some problems could arise owing to the interferences between the incident and the reflected microwaves. This fact cannot be verified with an accelerometer.

4. AN EXAMPLE OF APPLICATION

Since the metallic materials are reflective for the microwaves, it is impossible to generate acoustic waves in this kind of material by means of the thermal effect caused by microwave absorption. However, if a thin layer of an absorbing material is put on the metallic surface (see Figure 6), it could be expected that the microwave irradiation of this layer leads to the

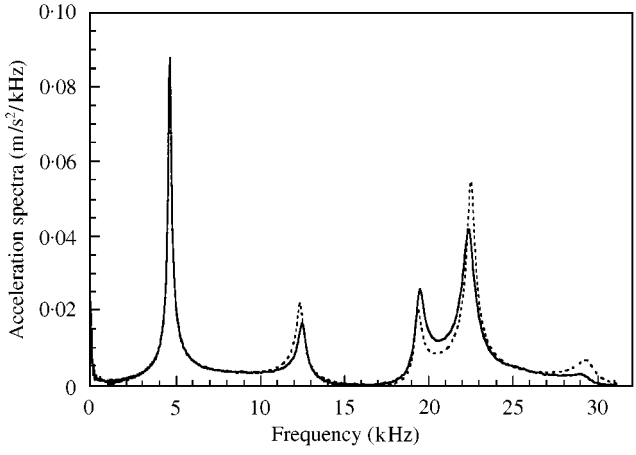

Figure 5. Experimental (——) and theoretical (·····) acceleration spectra.

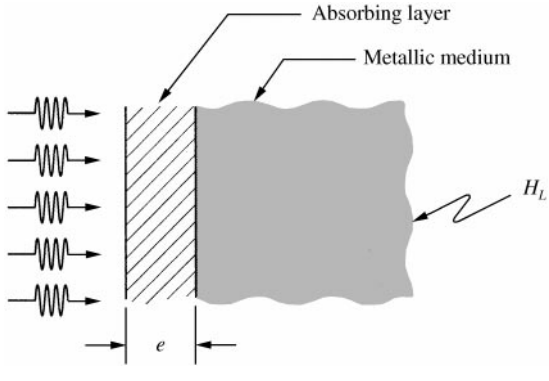

Figure 6. Microwave irradiation of an absorbing layer.

production of acoustic waves propagating in the metallic medium. This fact has been shown experimentally by Hosten and Bernard by irradiating a painted aluminium surface [8].

The aim of this section is to predict theoretically the acoustic waves generated at the interface between a thin absorbing layer and a metallic medium. The displacement of the free irradiated surface of the layer will be predicted too. Since a large surface can be irradiated with microwaves, the one-dimensional problem can be treated (uniaxial strain state). As an example, the layer, having a thickness e, is made of PVC and the metallic medium is an aluminium alloy plate. It will be assumed that the temperature rise in the PVC layers is uniform and the maximum temperature rise equals the value which has been measured in the previous section (8×10^{-5}°C). The temperature rise is given by equation (23). Since one is only interested in the acoustic waves generated by the absorbing layer (but not in the wave reflections in the metallic plate), it will be supposed in the calculations that the aluminium medium is semi-infinite. Consequently, the function H_L is given by

$$H_L = \mathrm{i}\rho_{Alu} A_{Alu}/\omega S^*_{Alu}. \tag{25}$$

The calculations have been performed for two different thicknesses of the PVC layer ($e = 0{\cdot}5$ and 1 mm). The displacements generated at the interface between the PVC layer

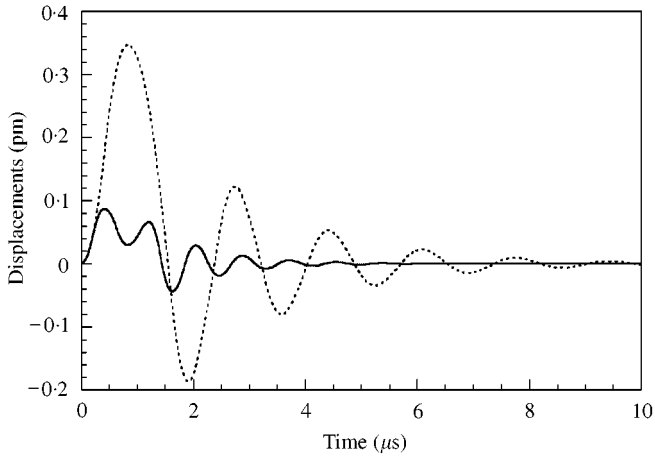

Figure 7. Displacements predicted at the interface between the PVC layer and the aluminium alloy medium. ——, $e = 0{\cdot}5$ mm; ·····, $e = 1{\cdot}0$ mm.

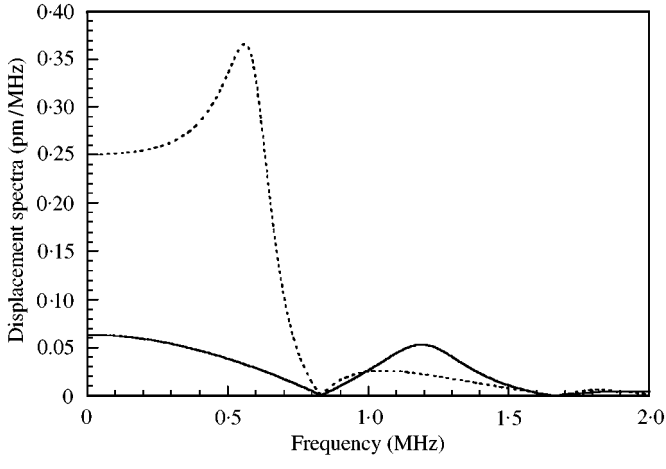

Figure 8. Displacement spectra predicted at the interface between the PVC layer and the aluminium alloy medium. ——, $e = 0{\cdot}5$ mm; ·····, $e = 1{\cdot}0$ mm.

and the aluminium alloy medium are plotted in Figure 7. The spectra of these displacements are plotted in Figure 8.

The results show that the amplitudes of the displacements are very small and that these amplitudes increase with the thickness of the layer. Consequently, the measurement of the displacement must be performed by means of a very accurate instrument (although the displacement at the free surface will be multiplied by two). In this case, the frequency range of the accelerometer is not convenient but some authors have shown that sub-picometer ultrasonic displacement amplitudes can be detected by a PZT piezoelectric transducer [13]. From equation (16), the displacements at the free surface of the polymeric layer ($z = 0$) have been calculated. The results are plotted in Figure 9.

At the free surface, the displacements are very much higher than at the interface between the two layers. This result could be expected since the mechanical impedance of the

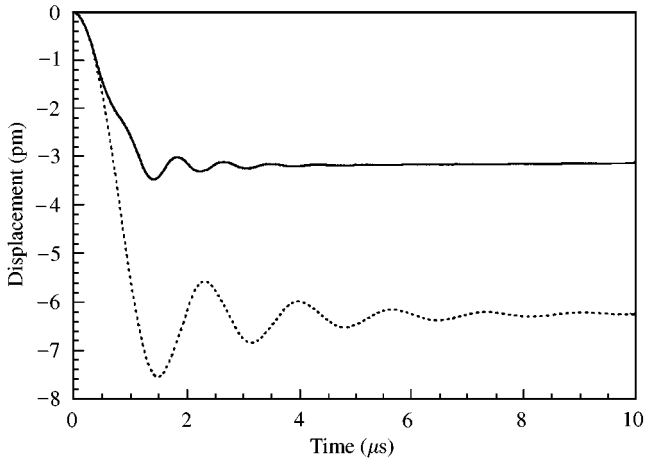

Figure 9. Displacements predicted at the free surface of the PVC layer. ——, $e = 0{\cdot}5$ mm; ·····, $e = 1{\cdot}0$ mm.

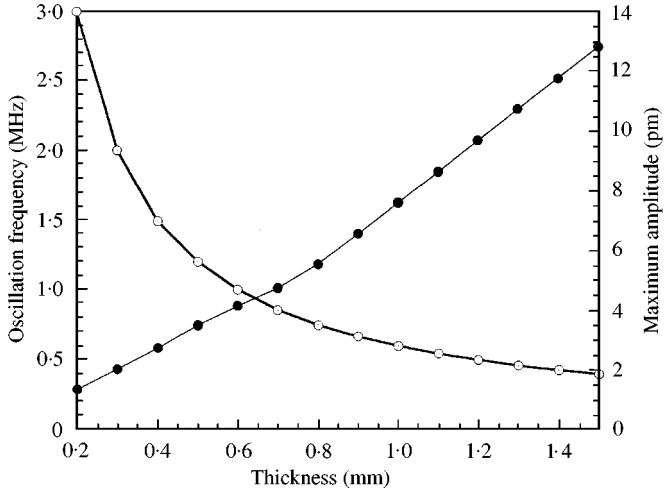

Figure 10. Displacement oscillation frequency and maximum amplitude versus layer thickness. —●—, Maximum amplitude; —○—, Oscillation frequency.

polymeric layer is less important that the impedance of the metallic medium. The oscillations visible in Figure 9 are related to the wave propagation in the irradiated layer.

If an accurate sensor has the ability to measure the displacement at the free surface without contact, one could imagine a new contactless method for the thickness measurement of layers. Although it is difficult experimentally, it seems that small high-bandwidth displacements, close to 1 pm, can be measured by optical interferometry [14–16]. In this method, the acoustic wave would be generated by electromagnetic microwaves. The main advantage of this method would be that tests could be performed in vacuum if necessary. For a PVC layer, in a thickness range from 0·2 to 1·5 mm, we have calculated the maximum amplitude of the displacement and the frequency of the displacement oscillations (with a maximum temperature rise of 8×10^{-5}°C). The curves are plotted in Figure 10. The knowledge of one of these curves permits the evaluation of the irradiated layer thickness.

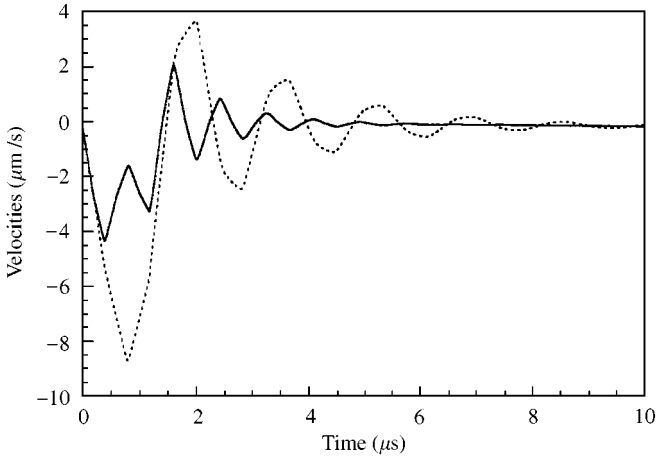

Figure 11. Velocities predicted at the free surface of the PVC layer. ——, $e = 0{\cdot}5$ mm; ·····, $e = 1{\cdot}0$ mm.

It is important to notice that the oscillation frequency does not correspond to the frequency of a free layer $\frac{1}{2}S'e$) since the presence of the metallic medium modifies this frequency. Indeed, the oscillation frequency is also related to the mechanical properties of the metallic layer. However, contrary to the maximum displacement amplitude, we have verified that the oscillation frequency does not depend on the temperature profile in the layer. For the layer thicknesses of 0·5 and 1 mm, the velocities of the free surface are plotted in Figure 11. It is shown that the order of magnitude of these velocities is close to 5 μm/s. According to the specifications of commercial Laser Doppler vibrometers, it seems that these velocities can be measured.

Since the generated displacements and velocities are quite difficult to measure in the configuration of the previous simulations, their amplitudes could be increased by different ways. For instance, the maximum temperature rise could be increased by using a more absorbing material, by increasing the power of the microwave generator or by increasing the pulsewidth. At the moment, a new microwave generator is being developed in order to increase the deposited energy in the irradiated medium.

5. CONCLUSIONS

A one-dimensional method has been presented to predict the acoustic waves generated by a rapid thermal expansion in a multilayer viscoelastic body made of any number of uniform layers when the temperature rise in each layer is known. With this method, any temperature profile can be investigated by dividing the body into a sufficient number of uniform segments with linear temperature profiles. The case of an exponential profile of the temperature rise has also been investigated.

An experimental validation has been performed on a rod made of two different materials (PVC and aluminium alloy), instrumented with an accelerometer and submitted to a time-gated microwave irradiation. In the frequency range of the accelerometer, the theoretical and the experimental acceleration spectra have been found to be very close.

An example of application has been carried out in the case of the acoustic wave generation in a metallic medium by means of the microwave irradiation of an absorbing layer. It has been shown that the amplitudes of the displacements generated at the interface

between a PVC layer and an aluminium medium are very small with the settings of the microwave generator used in the present study. The displacements at the free surface of the absorbing layer are more important. The simulations allow one to evaluate the amplitude of the generated waves and to study the measurement feasibility *a priori*. They help one to choose a suitable apparatus for the generation and the detection.

In the present paper, the temperature rise has been supposed or evaluated by comparing the theoretical and the experimental results. To complete the method, it would be interested to predict the temperature rise in the irradiated specimen from the electromagnetic properties of the materials and the characteristics of the incident microwaves. Then, the theory presented could be applied to predict the acoustic waves generated in an irradiated laminated composite plate in order to perform non-destructive evaluation or control for instance.

ACKNOWLEDGMENTS

The authors are indebted to the Conseil Régional d'Aquitaine and the Délégation Régionale à la Recherche et à la Technologie d'Aquitaine for their financial support.

REFERENCES

1. C. K. CHOU and A. W. GUY 1982 *Journal of the Acoustical Society of America* **71**, 1321–1334. Auditory perception of radio-frequency electromagnetic fields.
2. K. R. FOSTER and E. D. FINCH 1974 *Science* **185**, 256–258. Microwave hearing: evidence for thermoacoustic auditory stimulation by pulsed microwaves.
3. J. E. MICHAELS 1958 *Proceedings 3rd U.S. National Congress on Applied Mechanics*, 209–213. New York: American Society Mechanical Engineers,. Thermally induced elastic wave propagation in slender bars.
4. R. M. WHITE 1963 *Journal of Applied Physics* **34**, 3559–3567. Generation of elastic waves by transient surface heating.
5. L. S. GOURNAY 1966 *Journal of the Acoustical Society of America* **40**, 1322–1330. Conversion of electromagnetic to acoustic energy by surface heating.
6. D. E. BORTH and C. A. CAIN 1977 *IEEE Transactions on Microwave Theory and Techniques* **MTT-25**, 944–953. Theoretical analysis of acoustic signal generation in materials irradiated with microwave energy.
7. F. ENGUEHARD and L. BERTRAND 1997 *Journal of Applied Physics* **82**, 1532–1538. Effects of optical penetration and laser pulse duration on laser generated longitudinal acoustic waves.
8. B. HOSTEN and P. A. BERNARD 1998 *Journal of the Acoustical Society of America* **104**, 860–866. Ultrasonic wave generation by time-gated microwaves.
9. C. BACON, B. HOSTEN and P. A. BERNARD 1999 *Journal of the Acoustical Society of America* **106**, 195–201. Acoustic wave generation in viscoelastic rods by time-gated microwaves.
10. B. HOSTEN and C. BACON 2000 *Review of Progress in Quantitative Non Destructive Evaluation* **19**, 1113–1120. D. O. Thompson and D. E. Chimenti editors, Vol. 19, New York: Plenum Press, Measurement of complex Young moduli of composite materials by time-gated microwaves.
11. D. ROYER and E. DIEULESAINT 1983 *Ultrasonics Symposium Proceedings* **2**, 664–667. Influence of the elastic properties of the backing material in thermoelastic wave generation.
12. R. COULETTE, E. LAFOND, M. H. NADAL, C. GONDARD, F. LEPOUTRE and O. PÉTILLON 1998 *Ultrasonics* **36**, 239–243. Laser-generated ultrasound applied to two-layered materials characterization: semi-analytical model and experimental validation.
13. J. MOZINA and R. HROVATIN 1996 *Ultrasonics* **34**, 131–133. Detection of excimer laser induced sub-picometer ultrasonic displacement amplitudes.
14. D. VILKOMERSON 1976 *Applied Physics Letters* **29**, 183–185. Measuring pulsed picometer-displacement vibrations by optical interferometry.
15. A. J. HOLLOWAY and D. C. EMMONY 1988 *Journal of Physics E*: *Scientific Instruments* **21**, 384–388. Multiple-pass Michelson interferometry.

16. S. DILHAIRE, T. PHAN, E. SCHAUB and W. CLAEYS 1998 *Revue Générale de Thermique* **37**, 49–59. Sondes laser et méthodologies pour l'analyse thermique à l'échelle micrométrique. Application à la microélectronique.

APPENDIX A: NOMENCLATURE

a	axial acceleration
A	cross-sectional area of the irradiated body
C_{1k}^{*j}	components of the complex stiffness matrix in the orthotropic directions k in segment $\#j$
e	layer thickness
E^*	complex modulus
$\tilde{f}(z, \omega)$	Fourier transform of function $f(z, t)$ at cross-section z.
F	normal force
j	number of segments
L	length of the irradiated body
m	accelerometer mass
$\tilde{N}(\omega)$	Fourier transform of the strain at $z = 0$ due to the wave travelling in the direction of decreasing z
$\tilde{P}(\omega)$	Fourier transform of the strain at $z = 0$ due to the wave travelling in the direction of increasing z
$r(t)$	time shape of the temperature rise
S^*	complex slowness
t	time
u	axial displacement
v	axial particle velocity
z	axial coordinate
Z_a	accelerometer impedance
α_k^j	coefficients of linear thermal expansion in the orthotropic directions k of segment $\#j$
ε	longitudinal strain
ν	frequency
ω	angular frequency
ρ	mass density of the rod
σ	normal stress
τ	pulsewidth
θ	temperature rise